Synchronization of drift waves

D. Block* and A. Piel
Institut für Experimentelle und Angewandte Physik, Universität Kiel, Olshausenstrasse 40-60, 24098 Kiel, Germany

Ch. Schröder and T. Klinger
Institut für Physik, Universität Greifswald, Domstrasse 10a, 17489 Greifswald, Germany
(Received 20 September 2000; published 12 April 2001)

Based on a thorough experimental study of the equilibrium plasma state and the description of coherent drift modes in the framework of a linear, nonlocal model, the response of drift modes to different external driver signal is reported. Purely temporal perturbations as well as corotating and counter-rotating electric fields of various mode numbers are applied to the system. Drift mode synchronization and periodic pulling, typical for driven nonlinear oscillator systems, are investigated in detail. The full spatio-temporal behavior of periodic pulling is observed with multiprobe arrays.

DOI: 10.1103/PhysRevE.63.056401 PACS number(s): 52.35.Kt, 52.35.Mw

I. INTRODUCTION

The nonlinear dynamics of plasmas that leads to chaos [1] has attracted great interest during the last decade. Much effort has been spent to suppress chaotic states by simple feedback techniques [2,3] or by more sophisticated control techniques operating in phase space [4–7]. The successful control of oscillatory unstable plasmas suggests that, in near future, even weakly turbulent states of plasmas can be stabilized by externally applied perturbations. However, the development of such techniques requires a detailed understanding of the interaction between the involved plasma oscillations or waves and the applied signals. This is the motivation for conducting model experiments, which approach the goal step by step.

It is well known that the dynamics of a nonlinear, oscillatory unstable dynamical system with a periodic driving force exhibits peculiar features, e.g., quasiperiodicity [8] and period-doubling bifurcations towards chaos [9,10]. Furthermore, complete and incomplete synchronizations have been observed in various oscillatory unstable and periodically driven plasma experiments [11–15] and computer simulations [16,17]. The general concept of synchronization [8] turned out to be useful for many technical applications [18–20]. In this context synchronization means, among others, frequency entrainment, i.e., the oscillation frequency is shifted towards the frequency of the external driver. During incomplete synchronization the oscillation frequency is periodically pulled towards the external driver frequency but the coupling is too weak or the frequency mismatch is too large to establish complete synchronization. This concept is also known as periodic pulling [21] and is of great importance for the correct understanding of the dynamical behavior of various devices, such as unijunction transistor oscillator [22], microwave oscillator [18], neon bulb relaxation oscillator [23], and fluctuations in the earth's magnetosphere [24]. In laboratory plasmas periodic pulling has been subject of several investigations in recent years, e.g., beam-plasma systems [25–27], ion sound waves [28,29], potential relaxation oscillation [30–32], and grid sheath oscillation [11]. Hitherto, most investigations have focused on the temporal aspect of synchronization, but now the interest is shifting towards spatiotemporal behavior, including wave phenomena. At present, the understanding is most advanced for metastable-guided ionization waves in neon gas discharges [33]. It turned out that spatial and temporal periodic pulling is a fundamental feature of the transition between competing eigenmodes. Recent studies attacked the problem by application of a controlled spatiotemporal driving force [3]. However, the spatial component of spatiotemporal periodic pulling has not been directly observed in the described experiment.

The investigations presented in this paper deal with synchronization of drift waves. In the past, several attempts have been made to apply control signals to drift waves mainly by using feedback techniques [34,35]. Of central interest was the suppression of drift waves to achieve improved plasma confinement. The general nonlinear dynamics of the periodically driven system was paid less attention. One exception is the work of Lashinsky [21], where drift waves have been synchronized by applying an external driver signal to an electrode, placed inside the plasma column. The van der Pol model [36] was shown to give a qualitatively correct description of the observed dynamics.

Our experiments are based on application of a well-defined spatiotemporal driving force to synchronize drift waves. A multipole arrangement of electrodes is used to generate a propagating electric field structure.

The paper is organized as follows. We first discuss the plasma equilibrium and describe drift modes in the frame work of a linear, nonlocal model [37,38]. Next, we investigate the response of drift modes to various external signals, ranging from purely temporal perturbation to copropagating and counterpropagating electric fields of different mode numbers.

II. SPATIOTEMPORAL STRUCTURE OF COHERENT DRIFT WAVES

To study the effect of externally applied spatiotemporal electric fields on plasma dynamics, a careful description of

*Electronic address: block@physik.uni-kiel.de

TABLE I. Plasma and discharge parameters of the triple plasma device KIWI. *i-n* stands for ion-neutral collisions, *e-n* for electron-neutral collisions. Values with a radial dependence are taken in plasma center. L_n is taken at the position of maximum gradient.

Column length	$l=2$ m
Magnetic field	$B=0.07$ T
Argon gas pressure	$P=8\times10^{-4}$ mbar
e-n mean-free path	$\lambda_{en}=1$ m
i-n mean-free path	$\lambda_{in}=0.3$ m
Electron density	$n_e=(1-2)\times10^{16}$ m^{-3}
Electron temperature	$T_e=1.2$ eV
Ion temperature	$T_i\approx0.03$ eV
Density gradient length	$L_n=0.02$ m
Reduced gyroradius	$\rho_s=0.01$ m
Ion gyrofrequency	$\omega_{ci}=1.7\times10^5$ rad/s

the unperturbed situation is essential. After discussing the experimental setup we go into the details of the equilibrium plasma state and its relationship to drift wave dynamics.

A. Experiment KIWI

The experiments were conducted in the linear triple plasma device KIWI (Kiel Instrument for Wave Investigations) [39]. Two plasma source chambers are connected by a magnetized midsection where drift waves are observed. The magnetic field in the midsection can be regarded as homogeneous, except for the regions close to the grids, where the limited number of field coils causes diverging field lines. The plasma in the source chambers is produced by a thermionic hot-cathode discharge in steady-state operation with grounded anode. Confinement of primary electrons is enhanced by a multidipole magnetic configuration in line cusp geometry [40]. Both source chambers are equipped with magnetic compensation field coils to reduce magnetic mapping effects of primary electrons [41]. In the plasma column, electrons are well thermalized without any significant beam component. The confinement parameter β is low ($\beta\approx10^{-6}$) and the plasma is weakly ionized ($n_e/n_0\leqslant0.1\%$). The most important parameters are summarized in Table I.

The plasma source chambers are separated from the midsection by stainless-steel mesh grids with a transparency of 68%. For the present study, only one source chamber is operated. The separation grid at the active chamber is positively biased with respect to ground, while the other grid at the far end is always connected to ground. The grid bias acts as control parameter for destabilizing drift waves [42]. Depending on the grid voltage there are three distinct drift wave regimes. For low grid voltage (approximately 4 V), single drift modes are observed. For intermediate grid voltage (5–6 V) drift modes establish nonlinear saturation. Weakly developed drift wave turbulence is found for grid bias above 8 V. The transition from stability to weak turbulence follows the Ruelle-Takens-Newhouse scenario [43]. The subsequently described investigations are performed for intermediate grid voltage, i.e., in the region of saturated drift modes.

Cylindrical Langmuir probes (diameter, 0.2 mm and length, 5 mm) are used to measure equilibrium density profiles and local density fluctuations in the magnetized midsection [44]. Emissive probes are used to determine plasma potential profiles. Both probes are mounted on a two-dimensional positioning system to perform axial and radial scans through the plasma column. Langmuir probes are generally operated at positive bias with respect to local plasma potential and the current fluctuations are taken to be proportional to density fluctuations (it is reasonable to assume a nearly constant electron temperature). The azimuthal wave number is obtained with a circular 64-probe array [39].

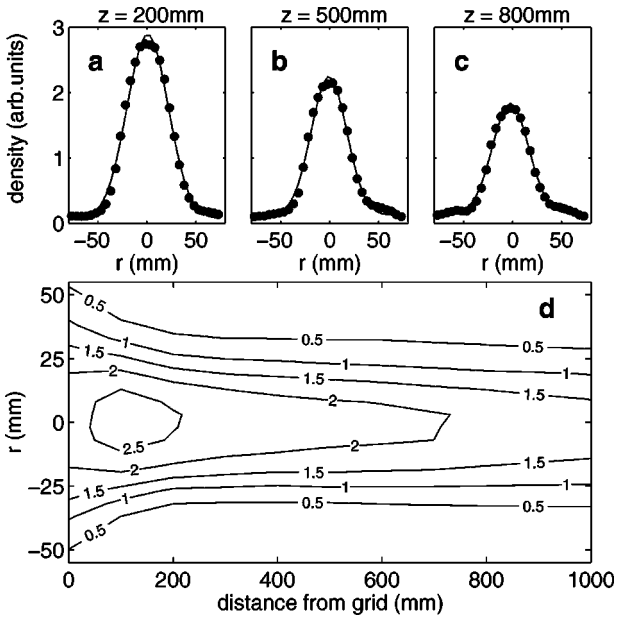

FIG. 1. (a)–(c) show radial density profiles at different axial positions. The solid line is a least square fit of a Gaussian to the measurement. The density contour (d) shows a 2D section through the center of the plasma column.

Throughout the paper we use a cylindrical coordinate system (r,z) with the z axis along the magnetic field and $z=0$ at the biased separation grid; $r=0$ is the center of the plasma column.

B. Plasma density

The radial pressure gradient is the driving mechanism for drift waves. Due to the fairly flat temperature profile we have $\nabla p_e=T_e\nabla n_e$. The plasma density profile is therefore of great importance and spatially resolved measurement of the plasma density in r and z direction are essential to characterize the global drift wave dynamics. The contour plot in Fig. 1(d) shows a typical density profile $n(r,z)$ of the KIWI device. Due to fringing magnetic field lines, the radial density profile is broadest near the grid and narrows within 200-mm distance from the grid. We believe that due to the convergence of the confining magnetic field lines the density maximum establishes at $z=100-200$ mm rather than close to the grid. Integrating $n(r,z)$ over r and θ shows that the plasma is injected at the grid and that the total number of charged particles in a plane perpendicular to z decreases along the z direction. The convergence of the magnetic field lines leads to a plasma density maximum at z

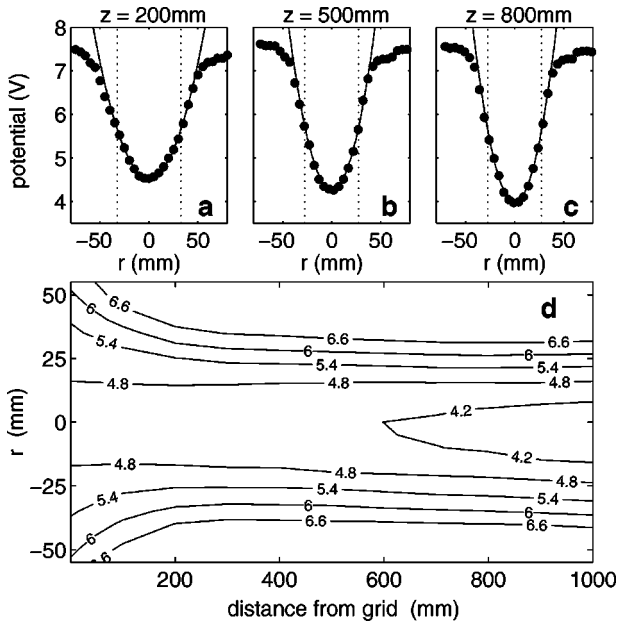

FIG. 2. (a)–(c) show radial plasma potential profiles at different axial positions. The solid line is a least square fit of a parabola to the measurement. The positions of maximum density gradient are marked with dotted lines. The potential contour (d) shows a 2D section through the center of the plasma column.

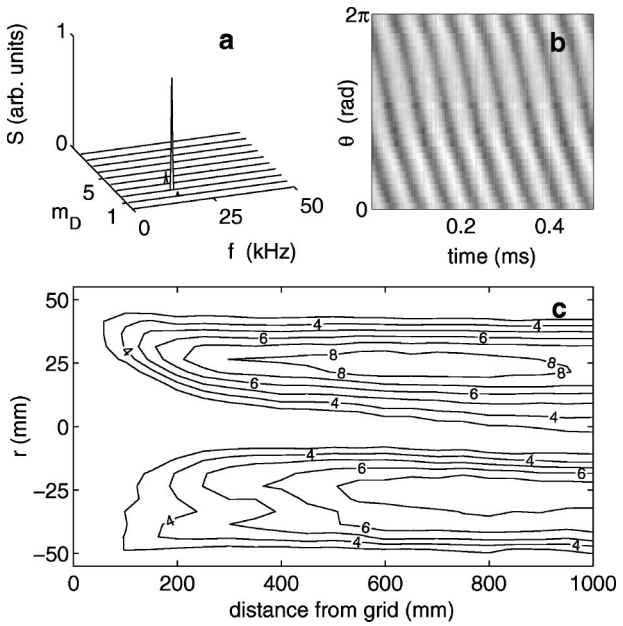

FIG. 3. (a) Frequency wave number spectrum of the $m=2$ drift mode. It has been calculated from the density fluctuation data shown in the gray-scale plot (b). The density fluctuation profile (c) is normalized with the the unperturbed density. The numbers attached to the contour lines are the density fluctuation amplitude in percent.

$=100–200$ mm although the total number of charged particles is lower than close to the grid. The density gradient for $z \geqslant 200$ mm is the result of axial and radial particle transport. The radial density profile at three different axial positions is plotted in Figs. 1(a–c). A least squares fit to the experimental data suggests that the radial density distribution is well approximated by a Gaussian $n(r) \propto \exp(-r^2/2r_p^2)$. The diamagnetic drift velocity is then given by

$$\mathbf{v}_{D,e} = -\frac{\nabla p_e \times \mathbf{B}}{qnB^2} = \frac{k_B T_e}{eB}\frac{r}{r_p^2}\mathbf{e}_\varphi , \tag{1}$$

with $\mathbf{e}_\varphi$ being the azimuthal unit vector. With the experimentally justified assumption of a radially constant electron temperature we find that the electron diamagnetic drift velocity is proportional to r only. The related drift frequency $\omega_{D,e} = v_{D,e}/r$ is independent of r, e.g., the drift is radially unsheared.

C. Plasma potential

Of similar importance is the plasma potential. Nonvanishing radial potential gradients cause azimuthal $E \times B$ drifts, which are known to be a destabilizing mechanism for drift waves [45]. A typical potential profile for the KIWI device is shown in the contour plot in Fig. 2(d). While the region close to the grid ($z < 200$ mm) is clearly dominated by fringing magnetic field lines, the region $z > 200$ mm is fairly uniform. The radial potential at three different axial positions is shown in Figs. 2(a–c). Close to the radial boundaries the plasma potential profiles are determined by sheath effects that are beyond the scope of the present study. We focus our discussion on the central part ($r \leqslant 40$ mm) of the the plasma column. This includes in particular the maximum density gradient region that is also the location of maximum drift wave amplitude [37]. The radial position of the maximum density gradient is indicated in Figs. 2(a–c) by dotted lines. The potential profile in the central plasma region is fitted by a parabola, justified by a simple magnetohydrodynamics (MHD) calculation that shows that a Gaussian density profile is self-consistent with a parabolic potential profile. Indeed, in the restricted region, $r \leqslant 40$ mm, a parabola fits the profile quite well (solid line). Using the parabolic potential profile, $\Phi_p = ar^2 + c$, we obtain an $E \times B$ velocity

$$\mathbf{v}_{E\times B} = \frac{\mathbf{E}\times\mathbf{B}}{B^2} = \frac{2ar}{B}\mathbf{e}_\varphi . \tag{2}$$

Again, we find that the drift velocity is proportional to r. Thus, the associated $E \times B$ frequency $\omega_{E\times B} = v_{E\times B}/r$ is independent of r.

D. Drift mode structure

Figure 3(a) shows the power spectrum $S(m,f)$ of a drift mode (mode number $m=kr$). The pronounced peak for $m=2$ indicates a single drift mode. Its azimuthal structure and propagation is visualized by a contour plot of time series recorded with the probe array [Fig. 3(b)]. Plasma densities fluctuations are gray-scale encoded. The phase velocity is in reasonable agreement with the linear theory. We note that there is an axial dependence of the electron diamagnetic drift and $E \times B$ drift. This introduces an axial shear of these drifts

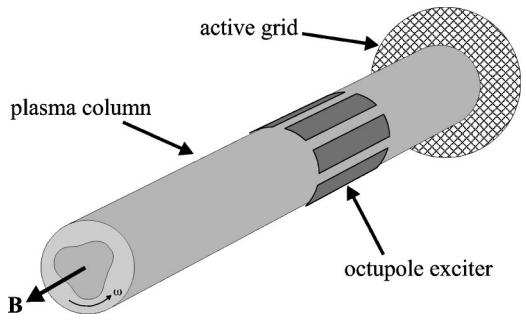

FIG. 4. Schematic drawing of the octupole exciter arrangement of electrodes with respect to the plasma column.

that is not considered in our simple analysis. That a global drift mode establishes despite of these axial inhomogeneities is shown in the fluctuation profile Fig. 3(c). The characteristic radial single humped eigenmode structure is found [37]. The axial mode structure comprises a standing wave (machine length $L=\lambda_{\parallel}/2$). Because this wave involves approximately equal distributions of the forward and reflected wave, simple phase measurements cannot determine the axial wave number. The slight difference in the absolute value of $k_{\parallel}$ for forward and reflected waves is introduced by axial inhomogeneities [38,46].

In summary the spatial structure of the drift waves in the KIWI device is rather well understood and can be related to the equilibrium profiles of the plasma. The presence of a global monochromatic drift mode makes it suitable for a systematic study of the influence of external driver signals on the drift wave dynamics.

III. SYNCHRONIZATION OF DRIFT WAVES

A. Experimental setup

The basic idea of controlling drift wave dynamics is based on the experience from other instabilities in plasmas where the electric field was found to be a good control parameter [47,48]. To apply rotating wave fields to the plasma, we use an octupole arrangement of electrodes (Fig. 4). Each electrode is 20 cm long and 2.5 cm wide. The radial position of the electrodes is carefully chosen to provide a reasonable contact to the plasma without acting as a limiter (Fig. 5). The

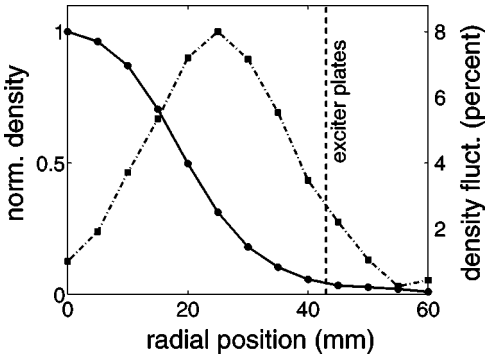

FIG. 5. Radial position of the exciter plates. For comparison the radial density profile (solid line) and the relative density fluctuation profile (dashed dotted line) are shown.

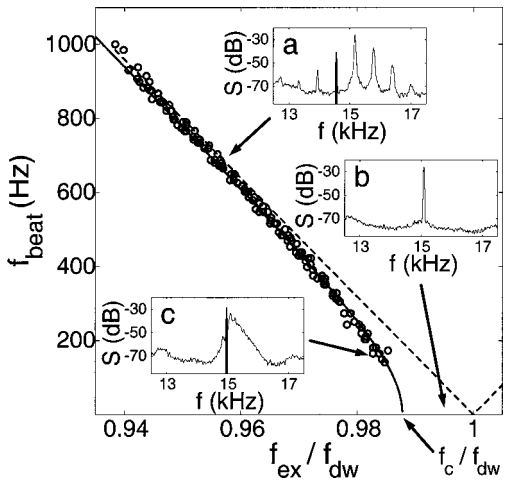

FIG. 6. Frequency dependence for a corotating exciter signal. The dashed line denotes the linear beat frequency $|f_{ex}-f_{dw}|$. f_c/f_{dw} marks the threshold above which synchronization takes place. (a) Modulation. Power spectrum for f_{ex} being smaller than f_c. The driver frequency peak is marked black. (b) Complete synchronization. Power spectrum for f_{ex} larger than f_c. (c) Incomplete synchronization. Power spectrum for $f_{ex}\approx f_c$. The driver frequency peak is marked black.

octupole exciter is axially placed at z=300 mm, i.e., close to the source chamber but within the region of homogeneous magnetic field. Each electrode is connected, via a power amplifier, to one of the outputs of an eight-channel digital synthesizer that generates (for each channel) a sinusoidal signal with an amplitude of a few volts peak to peak and frequencies $f_{ex}=0-30$ kHz. The phase shift between each channel can be controlled by software. With eight electrodes, it is possible to generate an azimuthal field structure with numbers $m_E=1-3$. The propagation direction of the exciter field can be chosen by the sign of the phase shift while the propagation velocity is determined by f_{ex}.

B. Temporal measurements

To investigate the interaction of the drift wave with the rotating exciter field, driver signals with different amplitude, frequency, sign of phase, and mode number have been applied. To simplify the presentation of the obtained results we introduce the following: f_{dw} represents the drift wave frequency observed without applied driver signal. The linear beating frequency is $f_{lb}=|f_{dw}-f_{ex}|$ while f_{nb} denotes the observed (nonlinear) beat frequency.

Figures 6 and 7 show the frequency dependence for co- and counter-rotating $m_E=2$ exciter signal applied to a $m=2$ drift mode, respectively. For small f_{ex}/f_{dw} ratio the power spectra show the signatures of simple amplitude modulation despite of the propagation direction of the exciter signal [Figs. 6(a) and 7(a)]. For corotating exciter signal the sideband structure is already more pronounced. If f_{ex}/f_{dw} is greater than a critical value f_c/f_{dw}, the drift mode is synchronized [Figs. 6(b) and 7(b)], whereby the critical value f_c strongly depends on the propagation direction. For corotating exciter signal f_c/f_{dw} is significantly smaller than for counter-rotating exciter signals. For f_{ex}/f_{dw} being a little

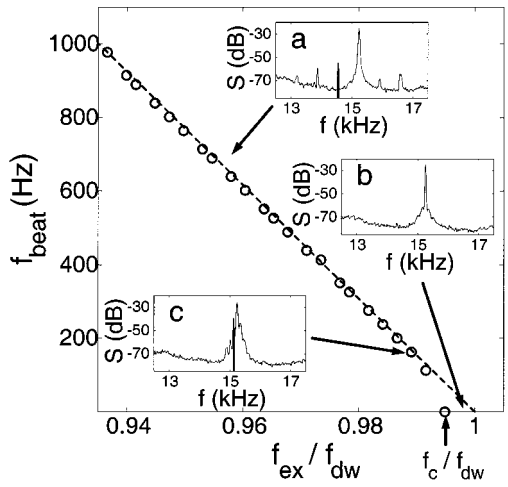

FIG. 7. Frequency dependence for a counter-rotating exciter signal. The notations are similar to those in Fig. 6. (a) Modulation. Power spectrum for f_{ex} being smaller than f_c. (b) Complete synchronization. Power spectrum for f_{ex} larger than f_c. (c) Modulation. Power spectrum for $f_{ex} \approx f_c$. A region of incomplete synchronization is not observed.

smaller than f_c/f_{dw} we find significantly different behavior for the two propagation directions. Simple modulation is observed for counter-rotating signals [Fig. 6(c)]. f_{nb} linearly decreases with increasing f_{ex} as f_{lb}, indicated by the dashed line. For corotating exciter signal, however, we observe a nonlinear dependence of f_{nb} on f_{ex}. The further f_{nb} deviates from the linear curve (dashed line), the more the sideband structure becomes asymmetric. Finally, we find a pronounced triangular shape [Fig. 7(c)].

To study the dependence between mode number and propagation direction of the exciter signal and the efficiency of synchronizing a drift mode, the width $|1-f_c/f_{dw}|$ [see Eq. (3)] is shown in Fig. 8 for a $m=2$ drift mode. Clearly, the synchronization of the $m=2$ drift mode is most efficient for matching mode number and propagation direction, which emphasizes the spatiotemporal character of our drift wave synchronization.

The observed synchronization for the other cases has to be interpreted as pure temporal synchronization effect, be-

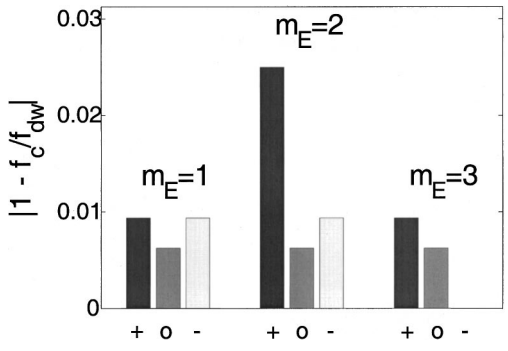

FIG. 8. Dependence of f_c on spatial exciter signal structure and propagation direction. The exciter signals have been applied to a $m=2$ drift mode. ''+'' denotes corotating exciter signal, ''−'' counter-rotating exciter signal, and ''O'' nonrotating exciter signal.

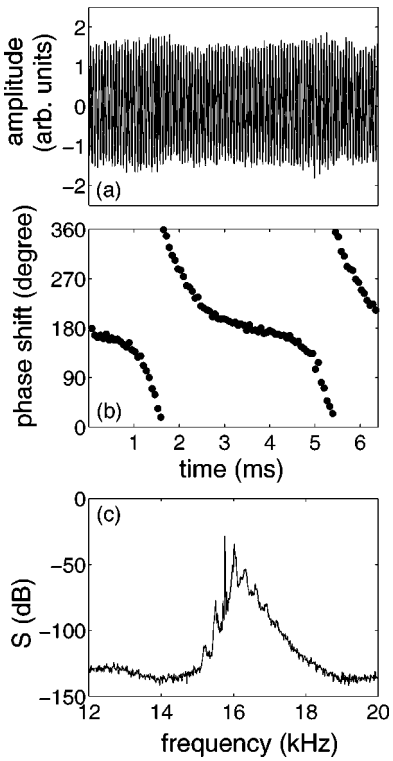

FIG. 9. Time development of (a) amplitude and (b) phase for an exciter signal with the same propagation direction and mode structure as the drift mode. (c) shows the power spectrum calculated from (a).

cause similar behavior is observed for only one active exciter plate.

The triangular shape of the power spectrum shown in Fig. 7(c) is a typical signature of periodic pulling, periodically repeated incomplete synchronization [21,22,49]. This is caused by simultaneous amplitude and phase modulation that leads to a nonlinear evolution of phase between exciter signal and drift wave response (Fig. 9). For many nonlinear plasma oscillations the driven van der Pol oscillator [36] gives a reasonable qualitative description. The nonlinear phase evolution with a fast and a slow time evolution is typical for a van der Pol-like behavior. The nonlinear dependence of f_{nb} from f_{ex} (Fig. 7) is described by

$$f_{nb} = f_{lb}\left(1 - \frac{f_c}{f_{lb}}\right)^{1/2}, \tag{3}$$

as derived from Adler's equation [50] that describes incomplete synchronization of nonlinear oscillators [22,32].

C. Spatiotemporal measurements

To study the spatiotemporal dynamics of incomplete drift wave synchronization a probe array is used [39]. With the signals from 15 probes distributed over half the circumference of the plasma column and taking the exciter signal applied to one plate as reference the spatiotemporal structure of the exciter signal and the drift wave is observed. Figure 10 shows the relative motion of a $m=2$ drift mode with respect

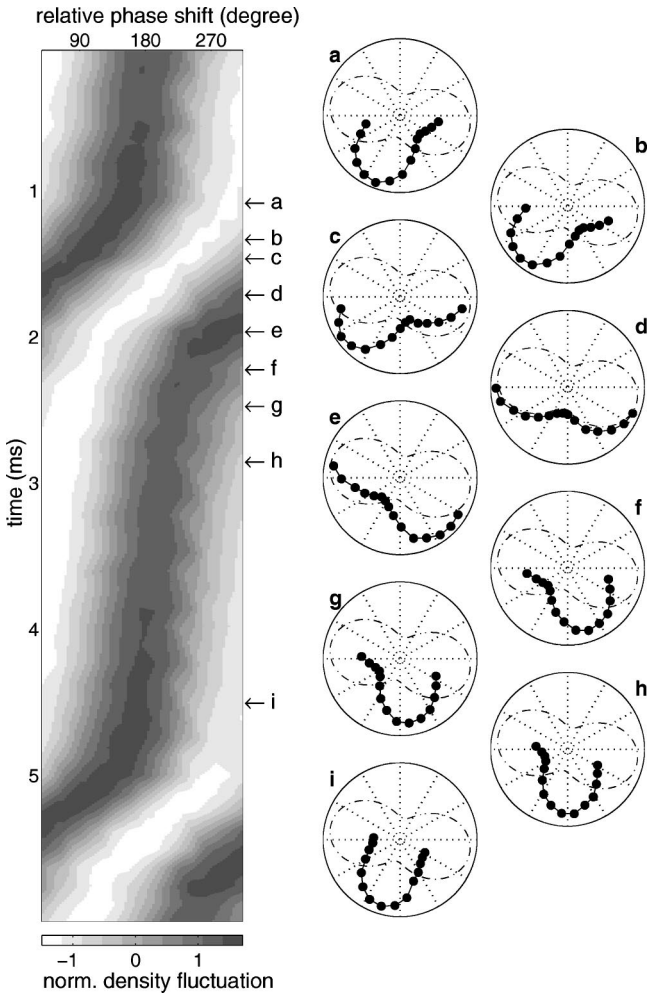

FIG. 10. Visualization of spatiotemporal periodic pulling. The gray-scale plot shows the time evolution of the $m=2$ drift mode phase with respect to the exciter signal. Typical for the process of periodic pulling are the two time scales. The polar plots (a)–(i) depict the relative motion of the drift mode (filled markers). The exciter signal is indicated by the dashed line. The maximum exciter signal belongs to positive potential while minimum exciter signal stands for negative potential. The drift mode maximum/maximum is related to positive/negative density fluctuations. (b)–(e) correspond to the fast-phase evolution and the drift mode maximum and exciter signal maximum have little phase shift. (f)–(i) belong to the slow-phase evolution and the drift mode maximum is close to the exciter signal minimum.

to a corotating $m_E=2$ exciter signal structure with $f_{ex}/f_{dw} \gtrsim f_c/f_{dw}$. In other words, Fig. 10 shows the drift wave in the rotating frame of the exciter signal. The temporal evolution of incomplete synchronization can be studied in the gray-scale plot. The phase is taken between the maximum density fluctuation relative to the position of the maximum exciter amplitude. Again we find time evolution on two different scales, a slow and a fast phase evolution, as already observed in the temporal analysis. However, this time the full spatiotemporal nature of periodic pulling is directly observed. [Figs. 10 (a–i)]. The dashed line is the exciter signal amplitude and the solid line and dots mark the drift wave. Comparison of gray-scale and polar plots reveals that the slow-phase evolution occurs where the phase shift is approximately 180°. The density maximum is then located at the potential minimum of the exciter signal [Fig. 10(h)]. The fast-phase evolution occurs when the drift wave density maximum is located at the potential maximum of the exciter signal amplitude [Fig. 10(d)]. As the density maximum of a drift wave is related to a positive potential fluctuation and the minimum of the exciter signal with negative potential, the 180° phase shift seems to be consistent within a electrostatic picture.

IV. SUMMARY AND DISCUSSION

Measurements of the global equilibrium plasma state in the KIWI device reveal axial inhomogeneities in density, potential, and in the magnetic field. The density gradient parallel to the magnetic field is just the signature of a source-sink plasma system. Nevertheless much of the drift wave behavior is unaffected by these inhomogeneities and the experimental arrangement is suitable for achieving a detailed understanding of the interaction of drift waves with external perturbation signals.

Temporal and spatiotemporal measurements demonstrate the possibilities of drift mode synchronization using an octupole arrangement of electrodes placed in the edge region of a magnetized plasma column. The efficiency depends on exciter frequency, mode number, propagation direction, and driver amplitude. Strongest interaction between drift mode and exciter field occurs, when the mode m_E of the exciter field and its propagation direction match the drift mode. This finding is in accord with former investigations on ionization waves [33], where wave-wave interaction was found to be much stronger than localized interaction. We find that resonant spatiotemporal excitation enhances interaction.

For exciter signals with a frequency close to the critical value, above which we find synchronization, periodic pulling is observed. Since periodic pulling is observed only with matching exciter mode numbers we conclude that the observed phenomenon of periodic pulling also depends on the spatial structure of the interaction. Spatio temporal measurements prove this. Observation of drift mode motion in the frame of the exciter signal visualizes the space-time evolution of the incomplete synchronization. Complete synchronization of the drift mode corresponds to a 180° phase shift. In the case of incomplete synchronization the drift mode almost locks to this phase. For a longer time interval it stays close to this favored state but, as the synchronization is not complete, it leaves this state after a while. The following motion through the unfavorable phase regime is fast. These two time scales are typical of the nonlinear process of periodic pulling. That the favored position is located at 180° phase shift suggests a simple electrostatic picture. As the maximum of the drift mode is related to a positive potential fluctuation and the minimum of the exciter signal amplitude with negative potential, the 180° position seems to be energetically favored. On the other hand, recent simulations [51] show that synchronization of drift waves can be obtained by assuming a system of field-aligned ac currents.

With respect to the present goal of controlling turbulent

plasma states, the results mark an important step in this direction. It was possible to carefully investigate in detail the interaction of drift waves and external applied exciter signals. The width of the synchronization region is found to be a valuable measure for the comparison of different scenarios. Further investigations are required on the interaction mechanism, its influence on anomalous transport, and basic processes of nonlinear dynamics. It was recently shown that this control method is capable to synchronize selected drift modes in a weakly turbulent plasma state [51].

ACKNOWLEDGMENTS

This work was supported by Deutsche Forschungsgemeinschaft under Contract No. Pi 185/14-1. The technical assistance of V. Rohwer is gratefully acknowledged.

[1] T. Klinger, in *Handbook of Chaos Control*, edited by H.G. Schuster (Wiley-VCH, Weinheim, 1998), pp. 513–562.
[2] A.K. Sen, Phys. Plasmas **7**, 1759 (2000).
[3] K.-D. Weltmann, M.E. Koepke, and C.A. Selcher, Phys. Rev. E **62**, 2773 (2000).
[4] T. Pierre, G. Bonhomme, and A. Atipo, Phys. Rev. Lett. **76**, 2290 (1996).
[5] T. Mausbach *et al.*, Phys. Lett. A **228**, 373 (1997).
[6] E. Gravier, X. Caron, and G. Bonhomme, Phys. Plasmas **6**, 1670 (1999).
[7] K.D. Weltmann, T. Klinger, and C. Wilke, Phys. Rev. E **52**, 2106 (1995).
[8] C. Hayashi, *Nonlinear Oscillations in Physical Systems* (Princeton University Press, Princeton, NJ, 164).
[9] U. Parlitz and W. Lauterborn, Phys. Rev. A **36**, 1428 (1987).
[10] R. Mettin, U. Parlitz, and W. Lauterborn, Int. J. Bifurcation Chaos Appl. Sci. Eng. **3**, 1529 (1993).
[11] H. Klostermann, A. Rohde, and A. Piel, Phys. Plasmas **4**, 2406 (1997).
[12] T. Klinger, F. Greiner, A. Rohde, and A. Piel, Phys. Plasmas **2**, 1822 (1995).
[13] H. Amemiya, Plasma Phys. **25**, 735 (1983).
[14] R.H. Abrams, Jr., E.J. Yadlowsky, and H. Lashinsky, Phys. Rev. Lett. **22**, 275 (1969).
[15] M.E. Koepke *et al.* Geophys. Res. Lett. **21**, 1011 (1994).
[16] F. Greiner, T. Klinger, and A. Piel, Phys. Plasmas **2**, 1822 (1995).
[17] A. Rohde, H. Klostermann, and A. Piel, Phys. Plasmas **4**, 3933 (1997).
[18] K. Kurokawa, Proc. IEEE **61**, 1386 (1973).
[19] N. Minorski, *Nonlinear Oszillations* (Krieger, Malabar, FL, 1983).
[20] N. N. Bogoljubow and J. A. Mitropolski, *Asymptotische Methoden in der Theorie der nichtlinearen Schwingungen* (Akademie-Verlag, Berlin, 1965).
[21] H. Lashinsky, in *Symposium on Turbulence of Fluids and Plasmas*, edited by J. Fox (Polytechnic Press, New York, 1968), pp. 29–46.
[22] M.E. Koepke and D.M. Hartley, Phys. Rev. A **44**, 6877 (1991).
[23] T.E. Sheridan, M.E. Koepke, C.A. Selcher, and T.N. Good, Proc. SPIE **2039**, 158 (1993).
[24] H. Lashinsky, T.J. Rosenberg, and D.L. Detrick, Geophys. Res. Lett. **7**, 837 (1980).
[25] Y. Nakamura, J. Phys. Soc. Jpn. **25**, 1315 (1970).
[26] Y. Nakamura, J. Phys. Soc. Jpn. **31**, 273 (1971).
[27] T. Tsuru, J. Phys. Soc. Jpn. **40**, 548 (1976).
[28] B.E. Keen and W.H.W. Fletcher, J. Phys. D **3**, 1868 (1970).
[29] K. Ohe and S. Takeda, Jpn. J. Appl. Phys. **11**, 1173 (1972).
[30] P. Michelsen, H.L. Pécseli, J.J. Rasmussen, and R. Schrittwieser, Plasma Phys. **21**, 61 (1979).
[31] T. Gyergyek, M. Čerček, N. Jelić, and M. Stanojević, Phys. Lett. A **177**, 54 (1993).
[32] T. Klinger, F. Greiner, A. Rhode, M.E. Koepke, and A. Piel, Phys. Rev. E **52**, 4316 (1995).
[33] M.E. Koepke, T. Klinger, F. Seddighi, and A. Piel, Phys. Plasmas **3**, 4421 (1996).
[34] K.I. Thomassen, Nucl. Fusion **11**, 175 (1971).
[35] V.V. Arsenin and V.A. Chuyanov, Usp. Fiz. Nauk **123**, 83 (1977) [Sov. Phys. Usp. **20**, 736 (1977)].
[36] B. van der Pol, Philos. Mag. **43**, 700 (1922); **3**, 65 (1927).
[37] R.F. Ellis and E. Marden-Marshall, Phys. Fluids **22**, 2137 (1979).
[38] F.F. Chen, Phys. Fluids **8**, 752 (1965).
[39] A. Latten, T. Klinger, A. Piel, and Th. Pierre, Rev. Sci. Instrum. **66**, 3254 (1995).
[40] K.N. Leung, G.R. Taylor, J.M. Barrick, S.L. Paul, and R.E. Kribel, Phys. Lett. A **57**, 145 (1976).
[41] T. Pierre, G. Leclert, and F. Braun, Rev. Sci. Instrum. **58**, 6 (1987).
[42] T. Klinger, A. Latten, A. Piel, G. Bonhomme, and T. Pierre, Plasma Phys. Controlled Fusion **39**, 145 (1997).
[43] T. Klinger *et al.*, Phys. Rev. Lett. **79**, 3913 (1997).
[44] K. Hansen, T. Klinger, and A. Piel, Rev. Sci. Instrum. **65**, 2615 (1994).
[45] E. Marden-Marshall, R.F. Ellis, and J.E. Walsh, Plasma Phys. Controlled Fusion **28**, 1461 (1986).
[46] S. Tsai, R.F. Ellis, and F.W. Perkins, Phys. Fluids **15**, 345 (1972).
[47] N.O. Krahnstöver, F. Greiner, T. Klinger, and A. Piel, Phys. Lett. A **239**, 103 (1998).
[48] T. Mausbach, T. Klinger, and A. Piel, Phys. Plasmas **6**, 3817 (1999).
[49] T. Klinger, A. Piel, I. Axnäs, and S. Torvén, Phys. Scr. **56**, 70 (1997).
[50] R. Adler, Proc. IRE **34**, 351 (1946).
[51] Ch. Schröder *et al.* (unpublished).